

Metabolic dysregulation in the *Atp7b*^{-/-} Wilson's disease mouse model

Clavia Ruth Wootton-Kee^{a,1}, Matthew Robertson^b, Ying Zhou^{a,c}, Bingning Dong^a, Zhen Sun^a, Kang Ho Kim^a, Hailan Liu^d, Yong Xu^{a,d}, Nagireddy Putluri^a, Pradip Saha^a, Cristian Coarfa^b, David D. Moore^{a,c,1} , and Alli M. Nuotio-Antar^{d,1} 

^aDepartment of Molecular and Cellular Biology, Baylor College of Medicine, Houston, TX 77030; ^bDan L. Duncan Cancer Center, Baylor College of Medicine, Houston, TX 77030; ^cIntegrative Molecular and Biomedical Sciences Graduate Program, Baylor College of Medicine, Houston, TX 77030; and ^dDepartment of Pediatrics, Baylor College of Medicine, Houston, TX 77030

Contributed by David D. Moore, December 8, 2019 (sent for review August 18, 2019; reviewed by Ronald M. Evans and Mitchell A. Lazar)

Inactivating mutations in the copper transporter *Atp7b* result in Wilson's disease. The *Atp7b*^{-/-} mouse develops hallmarks of Wilson's disease. The activity of several nuclear receptors decreased in *Atp7b*^{-/-} mice, and nuclear receptors are critical for maintaining metabolic homeostasis. Therefore, we anticipated that *Atp7b*^{-/-} mice would exhibit altered progression of diet-induced obesity, fatty liver, and insulin resistance. Following 10 wk on a chow or Western-type diet (40% kcal fat), parameters of glucose and lipid homeostasis were measured. Hepatic metabolites were measured by liquid chromatography–mass spectrometry and correlated with transcriptomic data. *Atp7b*^{-/-} mice fed a chow diet presented with blunted body-weight gain over time, had lower fat mass, and were more glucose tolerant than wild type (WT) littermate controls. On the Western diet, *Atp7b*^{-/-} mice exhibited reduced body weight, adiposity, and hepatic steatosis compared with WT controls. *Atp7b*^{-/-} mice fed either diet were more insulin sensitive than WT controls; however, fasted *Atp7b*^{-/-} mice exhibited hypoglycemia after administration of insulin due to an impaired glucose counterregulatory response, as evidenced by reduced hepatic glucose production. Coupling gene expression with metabolomic analyses, we observed striking changes in hepatic metabolic profiles in *Atp7b*^{-/-} mice, including increases in glycolytic intermediates and components of the tricarboxylic acid cycle. In addition, the active phosphorylated form of AMP kinase was significantly increased in *Atp7b*^{-/-} mice relative to WT controls. Alterations in hepatic metabolic profiles and nuclear receptor signaling were associated with improved glucose tolerance and insulin sensitivity as well as with impaired fasting glucose production in *Atp7b*^{-/-} mice.

nuclear receptors | liver | copper

Wilson's disease is an autosomal recessive disorder with equal prevalence in males and females caused by mutations in the copper transporter *Atp7b*. The result is free copper concentrations that exceed the functional capacity of copper-binding proteins, causing oxidative stress, hepatic inflammation, steatosis, fibrosis, and cirrhosis (1). The variable clinical presentation of metabolic disorders in Wilson's disease patients has been attributed to differing environmental and genetic factors (2). Recent metabolomic analysis of serum from Wilson's disease patients identified unique signatures including enrichment in the tricarboxylic acid cycle, amino acid metabolism, choline metabolism, and oxidative stress pathways (3). In agreement with these findings, a Wilson's disease rat model of chronic copper feeding had alterations in serum metabolite profiles, including decreased serum glucose (4).

Nuclear receptors play a central role in the regulation of hepatic metabolism. Defects in nuclear receptor signaling and lipid metabolism have been identified in patients with Wilson's disease and in *Atp7b*^{-/-} mice (5–7). In accord with this, we found that activity of the nuclear receptors FXR, RXR α , HNF4 α , and LXR-1 decreased in livers of *Atp7b*^{-/-} mice (8). Additional results in humans [PPAR α (9, 10)] and mice [FXR (7, 8), LXR (5)] link metabolic

and nuclear receptor dysfunction to Wilson's disease. Whole-genome sequencing revealed differentially methylated regions for genes involved in lipid metabolism, including HNF4 α and RXR α targets, in Wilson's disease patients (11).

We sought to further define metabolic consequences of Wilson's disease, hypothesizing that *Atp7b*^{-/-} mice would exhibit an altered metabolic phenotype linked to changes in nuclear receptor signaling. Here, we describe an unexpected increase in whole-body glucose tolerance and insulin sensitivity coupled with decreased fasting glucose production in *Atp7b*^{-/-} mice. Metabolomic and transcriptomic profiles link these findings with alterations in nuclear receptor target gene expression.

Results

***Atp7b*^{-/-} Mice Are Protected from Diet-Induced Obesity.** In accord with expectations from Wilson's disease and previous reports (8), *Atp7b*^{-/-} mice on a C57BL/6J background showed elevated hepatic copper, but not iron, levels, which were associated with induction of metallothionein 2 (*Mt2*) expression (*SI Appendix, Fig. S1 A and B*). At the end of the study, *Atp7b*^{-/-} mice had elevated serum ALT, ALP, and bilirubin (total, direct, and indirect), and lower albumin; however, globulin level and the albumin/globulin ratio were unchanged, suggesting that liver function was not significantly impaired (*SI Appendix, Fig. S1 C–H*). Similar

Significance

Wilson's disease is an autosomal recessive disorder that results in accumulation of toxic levels of copper in the liver, which can lead to cirrhosis and liver failure. Emerging evidence suggests that hepatic metabolic processes are altered in Wilson's disease patients and Wilson's disease animal models. Our studies revealed an unexpected improvement in glucose tolerance and insulin sensitivity in a Wilson's disease mouse model (*Atp7b*^{-/-}) that correlate with activation of AMPK. These findings have the potential to uncover therapeutic options for patients with Wilson's disease, as well as for patients with metabolic disorders such as type 2 diabetes and fatty liver disease.

Author contributions: C.R.W.-K., D.D.M., and A.M.N.-A. designed research; C.R.W.-K., Y.Z., B.D., Z.S., K.H.K., H.L., P.S., and A.M.N.-A. performed research; C.R.W.-K., M.R., Y.X., N.P., P.S., C.C., D.D.M., and A.M.N.-A. analyzed data; and C.R.W.-K., D.D.M., and A.M.N.-A. wrote the paper.

Reviewers: R.M.E., Salk Institute for Biological Studies; and M.A.L., University of Pennsylvania.

The authors declare no competing interest.

Published under the PNAS license.

Data deposition: The data reported in this paper have been deposited in the Gene Expression Omnibus database, <https://www.ncbi.nlm.nih.gov/geo/> (accession no. GSE125637).

¹To whom correspondence may be addressed. Email: wootenke@bcm.edu, moore@bcm.edu, or antar@bcm.edu.

This article contains supporting information online at <https://www.pnas.org/lookup/suppl/doi:10.1073/pnas.1914267117/-DCSupplemental>.

First published January 10, 2020.

to *Atp7b*^{-/-} mice on a mixed genetic background, *Atp7b*^{-/-} mice had pleiomorphic nuclei, ballooned hepatocytes, and microsteatosis; however, significant inflammation was not apparent (*SI Appendix, Fig. S2*) (12).

There are conflicting reports of metabolic status in Wilson's disease patients (13, 14). We assessed differences in body weight and composition, as well as the response of *Atp7b*^{-/-} mice to a Western-type diet challenge. For metabolic phenotyping experiments, we chose to study male mice since female C57BL/6J mice have been reported to be protected from obesity and insulin resistance in comparison to males (15). Starting at 6 wk of age, *Atp7b*^{-/-} and wild-type (WT) mice were provided a normal chow or a high-fat, high-sucrose Western-type diet and weighed for 10 wk prior to metabolic phenotyping experiments. Body-weight gain over time, total fat mass, and epididymal white adipose tissue (eWAT) weight were moderately decreased in chow-fed *Atp7b*^{-/-} mice in comparison with WT littermate controls (Fig. 1*A*). On a Western diet (WD), body-weight gain was more blunted and endpoint total fat mass and liver and eWAT weights were reduced in *Atp7b*^{-/-} mice compared with WT mice (Fig. 1*A*). Lean body mass and kidney weight, representative of lean mass, did not differ between genotypes on either chow or WD (*SI Appendix, Fig. S3 A and B*).

The decreased adiposity exhibited by *Atp7b*^{-/-} mice suggested differences in energy balance between *Atp7b*^{-/-} and WT mice. Therefore, indirect calorimetry was performed simultaneously

with measurement of activity and food intake at a time point prior to significant differences in body weight. Total daily food consumption decreased for chow-diet-fed *Atp7b*^{-/-} mice compared with littermate WT controls due to decreased food consumption during the dark (active) cycle (*SI Appendix, Fig. S4 A and B*). Although respiratory exchange ratio (RER) did not differ during the light (inactive) cycle, RER was increased during the dark cycle, indicating enhanced carbohydrate oxidation for *Atp7b*^{-/-} mice vs. WT controls (*SI Appendix, Fig. S4C*). Both ambulatory *x*-axis (walking) and *z*-axis (rearing or jumping) activities increased, whereas total *X*-activity (walking and stereotypy) did not differ for *Atp7b*^{-/-} mice compared with WT controls (*SI Appendix, Figs. S4 D–F and S5*). Although locomotor activity profiles differed, VO₂ and energy expenditure (heat) did not differ between *Atp7b*^{-/-} mice and WT littermate controls (*SI Appendix, Fig. S4 G and H*). These results link the decreased body-weight gain of *Atp7b*^{-/-} mice primarily to decreased food intake, with an additional potential contribution from increased activity.

Decreased Hepatic Steatosis in *Atp7b*^{-/-} Mice. In accordance with previous reports (5, 6), parameters of lipid metabolism were altered in *Atp7b*^{-/-} mice. WD-fed WT animals had increased serum and hepatic cholesterol (CHOL), triglycerides (TG), and free fatty acids (FFA) (Fig. 1*B*). However, WD-fed *Atp7b*^{-/-} mice had decreased hepatic CHOL, TG, and FFA in comparison with WT

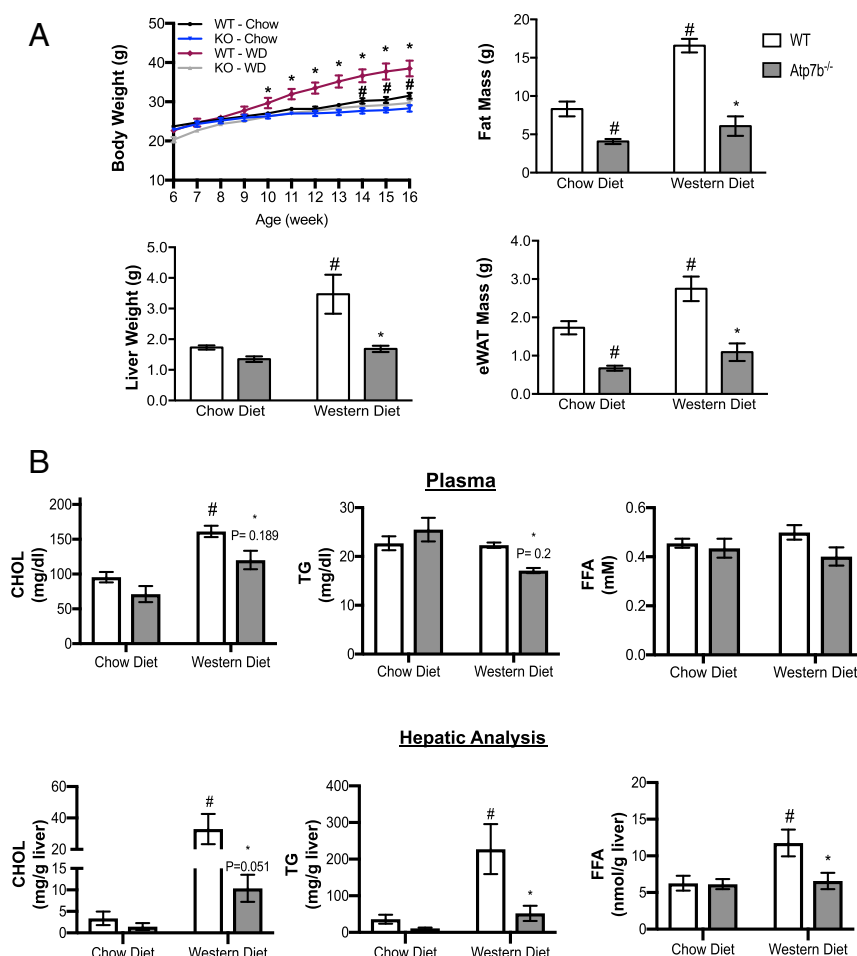


Fig. 1. Blunted weight gain and adiposity in *Atp7b*^{-/-} mice. (A) Body and liver weights, fat mass, and eWAT weights in *Atp7b*^{-/-} and WT mice on either chow or WD. (B) Plasma and liver tissue CHOL, TG, and FFA were measured. [#]*P* < 0.05 vs. WT chow diet; **P* < 0.05 vs. WT WD; two-way ANOVA, and Sidak's post hoc test. *n* = 4 to 11/group.

mice (Fig. 1B). Consistent with quantitative assessment of hepatic lipid content, Oil Red O staining showed decreased neutral-lipid staining for both the chow-fed and the WD-fed *Atp7b*^{-/-} mice relative to WT controls (SI Appendix, Fig. S6A). Oil Red O staining was also notable in nuclei of *Atp7b*^{-/-} mice on both diets (SI Appendix, Fig. S6). *Cd36* expression increased, suggesting that *Atp7b*-deficient hepatocytes take up more fatty acids (SI Appendix, Fig. S6B). However, in keeping with previous studies (7), both *Acadl* and *Mgl1* expression decreased, suggesting decreased beta oxidation, although *Cpt1a* expression was not different. *Ucp2* expression increased in *Atp7b*^{-/-} vs. WT control livers.

***Atp7b*^{-/-} Mice Are More Glucose Tolerant and Insulin Sensitive.** Glucose tolerance tests (GTT) revealed increased glucose tolerance in *Atp7b*^{-/-} mice fed chow diet in comparison with WT mice (Fig. 2A). Although the GTT curves did not differ between WD-fed *Atp7b*^{-/-} and WT mice, insulin levels in response to glucose injection decreased at all time points for WD-fed *Atp7b*^{-/-} mice in comparison to WT mice, suggesting enhanced insulin sensitivity in both chow and WD-fed *Atp7b*^{-/-} mice (Fig. 2B and C). Insulin tolerance tests (ITT) and homeostatic model assessment of insulin resistance (HOMA-IR) levels supported increased insulin sensitivity in both chow and WD-fed *Atp7b*^{-/-} mice (Fig. 2D–F). In accord with this, hyperinsulinemic euglycemic clamp studies showed increased glucose infusion rate and rate of disappearance of glucose (Rd) in *Atp7b*^{-/-} mice (Fig. 2G and H). This was accompanied by an increased metabolic index of glucose (Rg) (a marker of glucose uptake) in gastrocnemius muscle and eWAT in *Atp7b*^{-/-} mice (Fig. 2I and J). The endogenous rate of appearance of glucose (Ra), an index of endogenous glucose production, was not different between groups prior to or post insulin infusion (Fig. 2K). Consistent with enhanced glucose uptake, increased AMPK activation was observed in gastrocnemius muscle of chow-diet-fed *Atp7b*^{-/-} mice in comparison with WT controls (Fig. 2L).

Both chow- and WD-fed *Atp7b*^{-/-} mice exhibited striking hypoglycemia following insulin administration after fasting, with blood glucose levels dipping below 80 mg/dL by 15 and 45 min, respectively, suggesting an impaired glucose counterregulatory response (Fig. 2D and E) (16). Pyruvate tolerance tests (PTT) also indicated that fasted-state gluconeogenesis in *Atp7b*^{-/-} mice fed either chow or WD may be blunted relative to WT controls (Fig. 3A and B). Expression of glycogen synthase was significantly decreased in *Atp7b*^{-/-} relative to WT mice (SI Appendix, Fig. S7A). Although initial UDP-glucose measurements did not differ between groups, quantitative (colorimetric enzyme assays) and qualitative [periodic acid–Schiff (PAS) staining] methods demonstrated decreased hepatic glycogen content in ad-libitum-fed *Atp7b*^{-/-} vs. WT mice, reflecting a potential defect in synthesis and/or storage of glucose (SI Appendix, Fig. S7B–D). In contrast with normal hepatocytes, hepatocytes with abnormal morphology (ballooning with pleiomorphic nuclei containing inclusions) were unstained by PAS in *Atp7b*^{-/-} mice (SI Appendix, Fig. S7C). These results reveal that hepatic glucose production in the fasted state and glycogen stores may be decreased in *Atp7b*^{-/-} mice.

Hepatic AMPK Activation in *Atp7b*^{-/-} Mice. AMPK is activated in response to diverse cellular stresses, including increased reactive oxygen species (ROS) production. The well-established connection between excess intracellular copper and redox stress in WD suggested that hepatic AMPK activation could play a role in the metabolic phenotypes observed in *Atp7b*^{-/-} mice. Therefore, we measured total and phospho-AMPK in the liver. Chow-fed *Atp7b*^{-/-} mice did indeed have increased hepatic p-AMPK α , but not total AMPK, as shown by Western blot (Fig. 3C). In agreement with the expected impact of hepatic AMPK activation to decrease gluconeogenesis and lipogenesis, *Pepck1*, *Pcx*, *Fbp1*, *FASN*, *ACCI*, and *Srebp-1c* expression levels were reduced in *Atp7b*^{-/-} mice in comparison with WT controls (Fig. 3D and E).

Hepatic Metabolite Composition in *Atp7b*^{-/-} Mice. Analysis of the TCA cycle and glycolytic metabolic pathways revealed dramatic changes in hepatic metabolites. *Atp7b*^{-/-} mice had decreased hepatic glucose, pyruvate, and lactate levels; however, several glycolytic intermediates increased (G6P/F6P, 2PG/3PG, and PEP) (Fig. 4A). Similarly, there was an accumulation of TCA intermediates (oxaloacetate, citrate, fumarate, and malate), suggesting metabolic adaptation in the livers of *Atp7b*^{-/-} mice. Cancer metabolism and integrated stress-response studies have described a role for *Pepck2* (mitochondrial *Pepck*) in the promotion of cataplerotic mechanisms that promote “pyruvate recycling” as a mechanism for cell adaptation in conditions of stress (17, 18). Despite decreased *Pepck1*, *Pepck2* expression significantly increased in *Atp7b*^{-/-} mice (Fig. 4B). While the mechanism(s) for increased *Pepck2* in *Atp7b*^{-/-} mice are presently unclear, it is possible that copper-induced cellular stress is driving activation of endoplasmic reticulum-stress-mediated pathways previously shown to increase *Pepck2* (18).

In contrast, acetyl-CoA and α -KG decreased in *Atp7b*^{-/-} mice (Fig. 4A), which was accompanied by an increase in pyruvate dehydrogenase kinase 4 (*Pdk4*) and a decrease in pyruvate dehydrogenase α 1 (*Pdha1*) expression (Fig. 4C). Pyruvate dehydrogenase inactivation is reversed via dephosphorylation by the pyruvate dehydrogenase phosphatase enzyme (19). Together with increased *Pdk4* expression, the decreased *Pdpr* expression in *Atp7b*^{-/-} mice (Fig. 4C) may limit pyruvate flux into the TCA cycle. Furthermore, the changes in TCA cycle intermediates coincided with decreased *Mdh1* and succinate dehydrogenase complex (*Sdhb*) and increased *Idh2* gene expression (Fig. 4D).

Hepatic Transcriptomic Analysis and Predicted Transcription Factor Alterations in *Atp7b*^{-/-} Mice. Microarray transcriptomic analysis was performed with 3-mo-old WT and *Atp7b*^{-/-} mice (SI Appendix, Figs. S8 and S9), an age at which nuclear receptor dysfunction was detectable but livers lacked significant pathology (8, 12, 20). Kyoto Encyclopedia of Genes and Genomes (KEGG) pathway analysis showed that up-regulated pathways included proteasome, cell cycle, protein catabolism, oxidative phosphorylation, detoxification (glutathione metabolism), and TCA cycle. Pathways involved in immunity, calcium signaling, and synthesis of unsaturated fatty acids were down-regulated (SI Appendix, Fig. S9A). These findings are in keeping with transcriptomic studies in younger *Atp7b*^{-/-} mice on a mixed background and in Wilson’s disease patients (5, 6).

Furthermore, microarray data revealed significantly increased hepatic expression of the anorectic hepatokine *Gdf15* (SI Appendix, Table S1). Real-time PCR confirmed a fourfold increase in hepatic *Gdf15* expression for chow-diet-fed *Atp7b*^{-/-} mice at both 3 and 6 mo of age (SI Appendix, Fig. S10A). Serum GDF15 was also increased fourfold for chow-fed *Atp7b*^{-/-} mice at both 3 and 6 mo of age. Although Western diet feeding significantly increased serum GDF15 in WT mice, circulating GDF15 levels remained significantly greater in WD-fed *Atp7b*^{-/-} mice in comparison with WT controls (SI Appendix, Fig. S10B).

Transcription-factor-binding sites enriched within the regulatory regions of significantly changed gene sets were identified using EnrichR Analysis. As expected, nuclear-receptor-binding elements were strongly associated with down-regulated genes. In agreement with previous reports (7, 20), RXR α - and LXR α -binding sites were the most highly enriched in down-regulated genes, likely reflecting dysfunctional nuclear receptor activity (Fig. 5). LXR-binding elements were also enriched to a lesser extent in the up-regulated gene dataset. PPAR α elements, along with PXR (a xenobiotic detoxification nuclear receptor), were represented in the down-regulated gene data set. Transcriptomic analysis of decreased genes containing PXR-binding elements included *Cyp7b1* and *Elov2*, revealing a link between aberrant xenobiotic and lipid metabolism and lipogenesis (SI Appendix, Table S1).

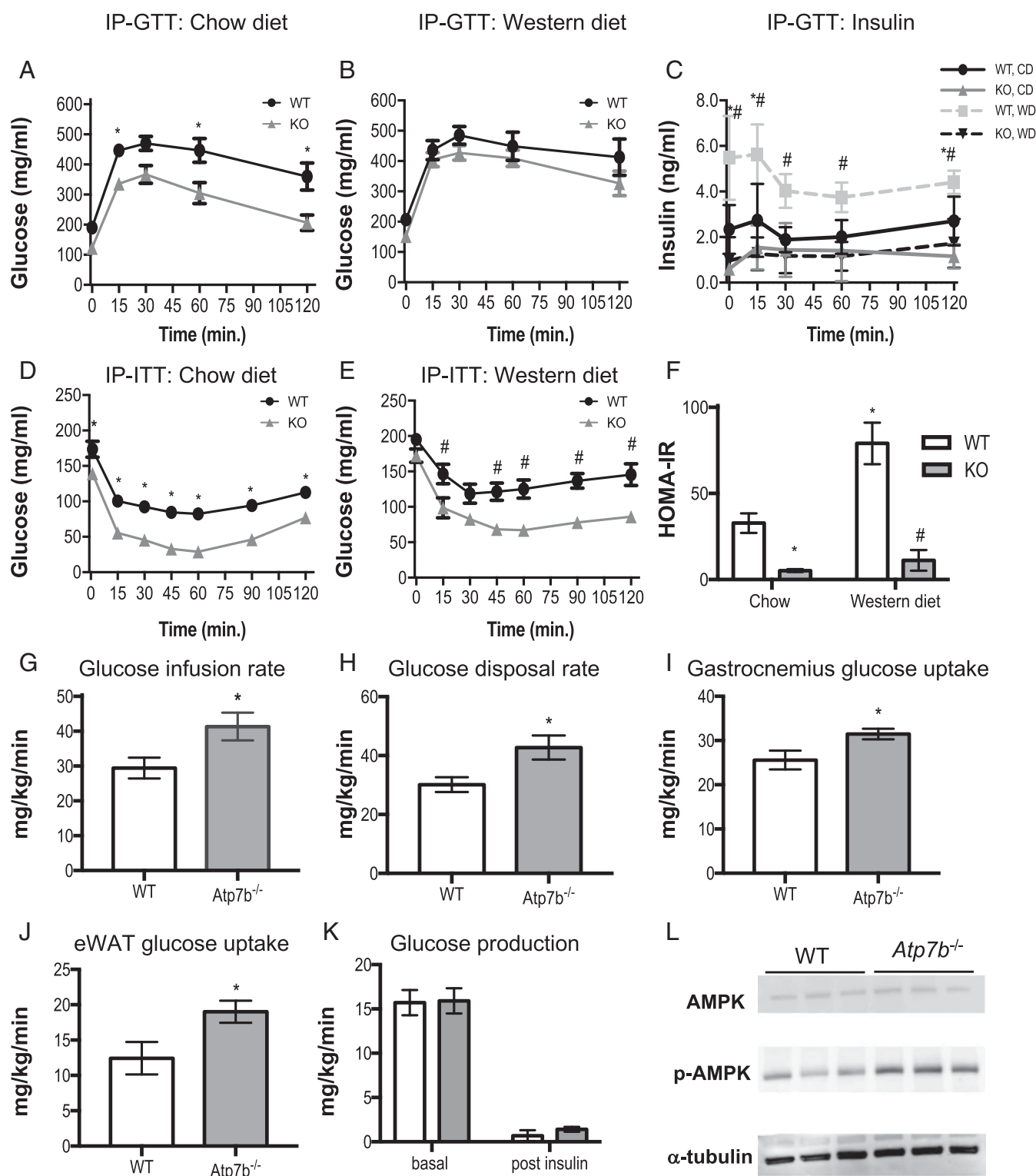


Fig. 2. Glucose tolerance and insulin sensitivity in *Atp7b*^{-/-} mice. (A and B) GTT. (C) Insulin released during intraperitoneal (IP)-GTT time course. (D and E) ITT was performed on 6-mo-old *Atp7b*^{-/-} and WT mice fed either (A and D) chow or (B and E) WD. (F) HOMA-IR. (G–K) Hyperinsulinemic euglycemic clamp was performed with 4- to 7-mo-old chow-fed *Atp7b*^{-/-} and WT mice. (L) Western blot analysis of gastrocnemius muscle AMPK and p-AMPK levels in chow-fed WT and *Atp7b*^{-/-} mice. (A–F) **P* < 0.05, WT vs. *Atp7b*^{-/-}, chow; #*P* < 0.05 WT vs. *Atp7b*^{-/-}, WD; two-way ANOVA, and Sidak's post hoc test. *n* = 4 to 11/group. (G–K) **P* < 0.05, Student's *t* test for *Atp7b*^{-/-} mice vs. WT; *n* = 5 to 6 mice/group.

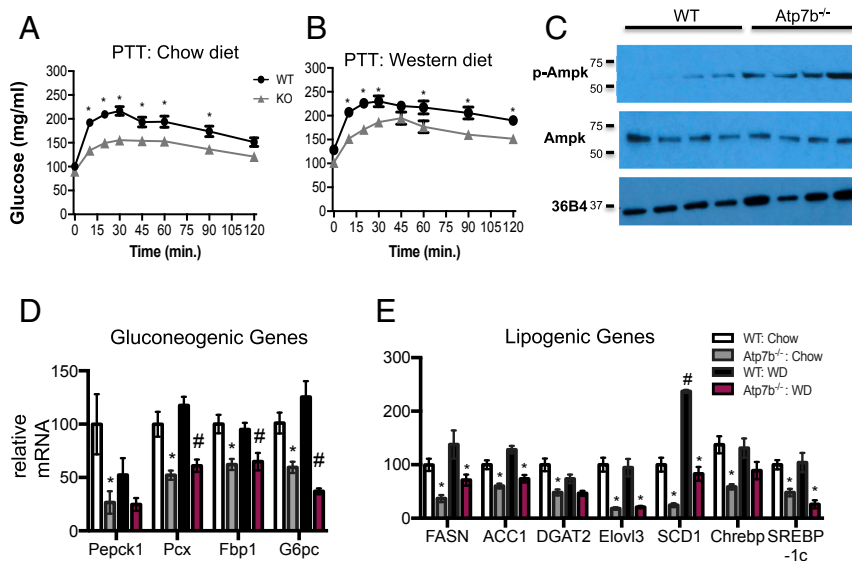


Fig. 3. Fasted-state gluconeogenesis and AMPK activation. (A and B) PTT on *Atp7b*^{-/-} and WT mice. (B) Western blot analysis of hepatic AMPK and p-AMPK levels in chow-fed 6-mo-old WT and *Atp7b*^{-/-} mice. (C) Hepatic gluconeogenic and (D) lipogenic gene mRNA expression measured by real-time PCR analysis. (A and B) **P* < 0.05, *Atp7b*^{-/-} vs. WT diet-matched control, two-way ANOVA, and Sidak's post hoc test. *n* = 4 to 11/group. (D and E) **P* < 0.05 vs. WT chow; #*P* < 0.05 vs. WT WD; Student's *t* test. *n* = 5 mice/group.

The most abundant transcription-factor-binding elements within the up-regulated genes were binding sites for FoxM1, E2F4, and androgen receptor (AR), which is consistent with cell-cycle pathway enrichment in the KEGG pathway analysis of the transcriptomic data (SI Appendix, Fig. S9B).

Discussion

Copper-mediated impairment of liver function is well characterized in Wilson's disease patients and in *Atp7b*^{-/-} animal models. The most commonly described dysfunctions in Wilson's disease patients are hepatic steatosis and cirrhosis. Surprisingly little is known regarding glucose and lipid metabolism in these patients, and the limited available case reports disagree regarding glucose tolerance in Wilson's disease patients (13, 14). Wilson's disease is a rare autosomal recessive disorder (1:30,000 occurrence), and this low incidence together with environmental and genetic variability likely contribute to the lack of a clear conclusion regarding glucose homeostasis in Wilson's disease patients (2). *Atp7b*^{-/-} mice provide a robust model for studying metabolism because environmental and genetic factors are more precisely controlled.

We measured multiple metabolic parameters in *Atp7b*^{-/-} mice and WT littermate controls maintained on either normal chow or Western-type diets. Chow-fed *Atp7b*^{-/-} mice exhibited modestly reduced adiposity and body weight by 14 wk of age. On WD, *Atp7b*^{-/-} mice exhibited more pronounced reductions in body weight, adiposity, and hepatic steatosis in comparison with WT. The reduction in hepatic steatosis may be secondary to reduced obesity observed for WD-fed *Atp7b*^{-/-} mice in comparison with WT littermate controls. *Atp7b*^{-/-} mice ate less food and were more active, which may implicate a central component in the observed metabolic differences. Indeed, our microarray and real-time PCR data revealed a fourfold increase in hepatic *Gdf15* expression for chow-diet-fed *Atp7b*^{-/-} mice in comparison with WT controls at 3 mo of age, prior to observed weight differences, and continuing through 6 mo of age. *Gdf15* has recently emerged as an inhibitor of food intake (21), suggesting that this anorectic hepatokine may contribute to decreased food intake observed in *Atp7b*^{-/-} mice. Serum *Gdf15* levels were similarly elevated for chow-fed *Atp7b*^{-/-} mice of both age groups. Western

diet feeding increased serum *Gdf15* levels in WT mice, with even higher levels in *Atp7b*^{-/-} mice (SI Appendix, Fig. S10).

Our findings support previous reports of decreased hepatic and serum lipids in mixed-background *Atp7b*^{-/-} mice (5, 6). However, significantly decreased hepatic and fasting plasma lipid levels relative to WT were evident only for *Atp7b*^{-/-} mice when they were fed WD. This may reflect altered genetic susceptibility to lipid synthesis, oxidation, and accumulation among mouse strains since *Atp7b*^{-/-} mice on WD did have decreased serum and hepatic cholesterol and triglyceride levels in comparison with WT mice.

In previous studies, white adipose tissue (WAT) in mixed-background *Atp7b*^{-/-} mice showed a correlation between copper levels and lipolysis in explant WAT (22), and copper levels were inversely correlated with steatosis in nonalcoholic fatty liver disease (NAFLD) patients (23, 24) and rodent NAFLD models (25, 26). While we did not observe an effect on fasting-plasma free fatty acids, it remains to be determined whether the decreased adiposity observed in *Atp7b*^{-/-} mice on the C57BL/6 background is in part due to a primary alteration in adipocyte function or to a secondary effect of copper accumulation in the liver or elsewhere. Interestingly, hepatocyte-specific knockout of *Atp7b* (*Atp7b*^{ΔHep}) resulted in increased adiposity and weight gain despite limited hepatic inflammation, possibly due to alterations in cell signaling in nonparenchymal cells and to increased metallothionein expression (copper chelation) in *Atp7b*^{ΔHep} mice (27). Furthermore, *Atp7b*^{-/-}, but not *Atp7b*^{ΔHep}, mice have abnormal enterocyte morphology, accumulation of enteric lipid droplets, and disrupted chylomicron assembly (28), which may account for differences in metabolic phenotype between *Atp7b*^{-/-} and *Atp7b*^{ΔHep} mice.

Recent findings in an *Atp7b*^{-/-} rat model (cross breed between the Long-Evans-Cinnamon rat and the Piebald Virol Glaxo rat, defective in pineal night-specific ATPase [PINA] and *Atp7b* [LPP rat]) demonstrated increased visceral fat, hepatic triglyceride content, liver weight, and macrosteatosis in response to a high-calorie diet (45% kcal from fat and 722 kcal/L fructose-supplemented drinking water), which correlated with increased hepatic mitochondrial damage (29). In contrast with *Atp7b*^{-/-} mice, LPP rats did not have aberrations in visceral fat or other parameters of lipid metabolism on a normal diet (29). There are potential genetic and physiologic reasons underlying these differences. The PINA gene is

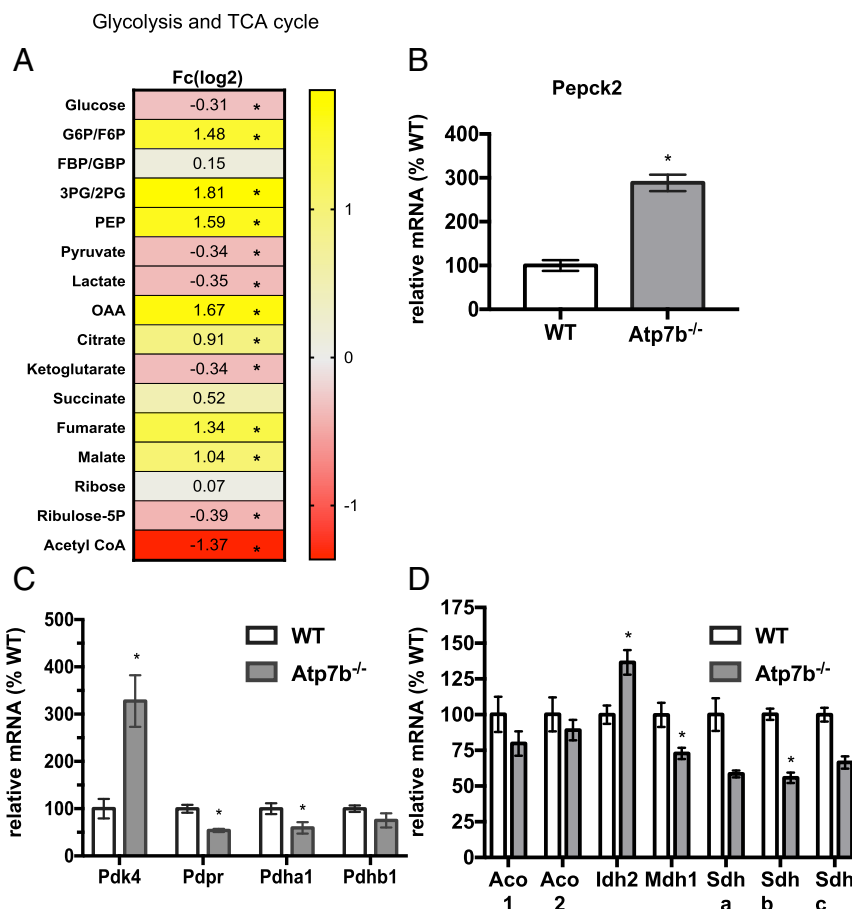


Fig. 4. Hepatic metabolic changes in *Atp7b*^{-/-} mice. (A) Hepatic glycolytic/TCA cycle metabolites significantly changed (B) hepatic *Pepck2* mRNA, (C) hepatic regulators of the pyruvate dehydrogenase complex, and (D) hepatic TCA cycle genes. (A) Student's *t* test followed by false discovery rate (FDR) correction; **q* < 0.25. *n* = 4 to 7 mice per group. (B–D) *n* = 5 to 11 mice per group. Student's *t* test was used to determine differences between *Atp7b*^{-/-} mice vs. WT controls; **P* < 0.05 vs. WT.

expressed from an intronic promoter within the *Atp7b* gene and is deleted in the LPP rat but not the *Atp7b*^{-/-} mouse (30). Given the important role of circadian rhythm in metabolism, circadian disruptions arising from defective PINA activity may contribute to different metabolic outcomes between LPP rats and *Atp7b*^{-/-} mice. Furthermore, LPP rats develop fulminant liver failure followed by death, such that untreated animals die between 90 and 120 d of age, whereas *Atp7b*^{-/-} mice are longer-lived (31). The basis for this difference in disease progression is unclear since both animal models have similar levels of hepatic copper accumulation.

GTT, ITT, hyperinsulinemic euglycemic clamps, and skeletal muscle AMPK activation demonstrated increased glucose tolerance and insulin sensitivity in *Atp7b*^{-/-} mice. However, marked hypoglycemia during ITTs, as well as PTT data, also supported a defective counterregulatory response. Gene expression data indicate marked down-regulation of gluconeogenic genes in livers of *Atp7b*^{-/-} mice, and glycogen storage and glycogenesis may also be reduced in *Atp7b*^{-/-} mice, suggesting that glucose production may be impaired in patients with Wilson's disease and render them more susceptible to episodes of hypoglycemia when fasting, particularly under conditions of increased non-glucose-stimulated insulin secretion. Thus far, one published case study has reported hypoglycemia, which resolved with treatment, in a patient diagnosed with Wilson's disease (32). Furthermore, cirrhosis is often observed in Wilson's disease patients and is frequently associated with aberrant nutritional status. Patients with liver cirrhosis may present with hypocholesterolemia, impaired absorption of fat-soluble

vitamins, glycogen storage disorders, impaired gluconeogenesis, and increased catabolism (33). Therefore, the improved glucose tolerance in *Atp7b*^{-/-} mice may reflect progressive liver damage, rather than a component of normal/healthy metabolism, due to effects on glucose production. Our results suggest an impaired glucose counterregulatory response as a potential mechanism for hypoglycemic episodes in the context of *Atp7b* deficiency.

The metabolic aberrations that we observed in *Atp7b*^{-/-} mice are consistent with impaired nuclear receptor activity. Expression of *Ppara* and of many of its targets decreased in *Atp7b*^{-/-} vs. WT mice. *Atp7b*^{-/-} mice had impaired expression of several FXR-regulated gluconeogenic target genes, in agreement with reduced FXR activity in this mouse model (7, 8). Analysis of transcription-factor-binding sites upstream of differentially regulated genes suggested increased AR activity. Classical ligand-dependent activation of AR has been shown to be protective against NAFLD and insulin resistance in male mice (34), whereas nonligand-dependent activation of AR via MAPK signaling has been shown to promote hepatocarcinogenesis (35). Furthermore, reduced gluconeogenic capacity and hepatic glycogen synthesis are in keeping with reduced glucocorticoid receptor (GR) and circulating glucocorticoid levels observed for *Atp7b*^{-/-} mice (7). GR expression and activity have been reported to be directly controlled by FXR activity, influencing hepatic gluconeogenic responses in the fasted state in mice (36). Further chromatin immunoprecipitation sequencing (ChIP-seq) analysis in *Atp7b*^{-/-} and control livers is necessary to

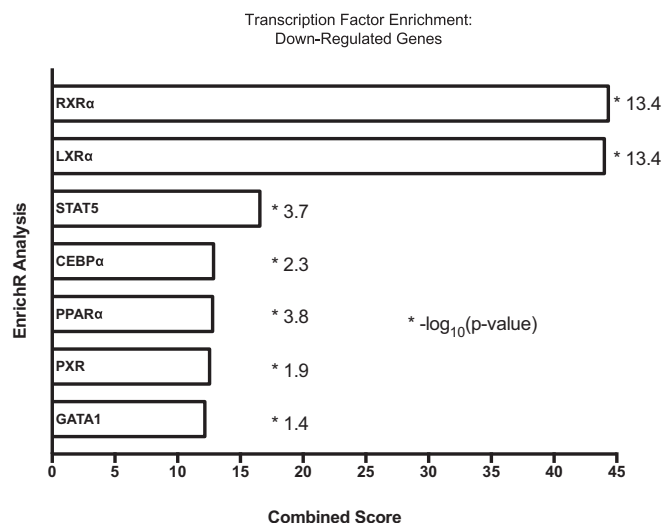


Fig. 5. Transcriptomic analysis in *Atp7b*^{-/-} mice livers. Pathway analysis of transcription factor binding was performed with the significantly changed microarray analysis genes ($F_c > 1.5$, $FDR < 0.05$) using the web-based EnrichR platform (27141961). Binding sites identified from ChIP-Seq data within the following down-regulated genes: RXR(NR2B1)_22158963_ChIP-Seq_LIVER_Mouse; LXR(NR1H3)_22158963_ChIP-Seq_LIVER_Mouse; STAT5_23275557_ChIP-Seq_MAMMARY-EPITHELIUM_Mouse; CEBPα_23403033_ChIP-Seq_LIVER_Mouse; PPARα(NR1C1)_22158963_ChIP-Seq_LIVER_Mouse; PXR(NR1I2)_20693526_ChIP-Seq_LIVER_Mouse; GATA1_22025678_ChIP-Seq_K562_Human. * $-\log_{10}(P \text{ value})$.

determine the broad patterns of nuclear-receptor binding in response to increased copper load.

Increased hepatic AMPK activation may be responsible for reduced gluconeogenic and lipogenic gene expression. AMPK serves as a sensor of energy status, as well as cellular stress (such as ROS production) (37–40). Copper-induced production of ROS production is well characterized in Wilson's disease patients and animal models (2) and may provide a stimulus for AMPK activation in *Atp7b*^{-/-} mice. Alternatively, AMPK is activated in response to UCP2-mediated depletion of cellular ATP (41, 42). Ucp2 has been identified as a transcriptional target of both FOXM1 (43) and E2F4 (44, 45), the transcription factors with the two most highly up-regulated binding sites identified in our study. FOXM1 expression has been reported to be up-regulated by GDF15, activated by oxidative stress, and to negatively regulate expression of the copper transporter *Ctr1*, suggesting that FoxM1 may play a larger role in mediating the cellular response to excess copper (46, 47). Future studies will investigate the underlying mechanisms for AMPK activation and the impact on metabolism in *Atp7b*^{-/-} mice in relation to ROS generation.

Decreased gluconeogenesis, hepatic glucose, pyruvate, and lactate concentrations were accompanied by a significant increase in glycolytic intermediates, as well as unexpected increases in many TCA cycle intermediates despite decreased Ac-CoA. In support of decreased TCA cycle metabolic flux, we found increased Pdk4 mRNA expression. Future studies measuring TCA cycle flux are necessary to determine the mechanism for increased TCA cycle intermediates.

Here we describe metabolic changes in *Atp7b*^{-/-} mice that are likely a consequence of impaired hepatic nuclear receptor function. We observed dramatic alterations in glucose homeostasis, metabolome, and AMPK activation in *Atp7b*^{-/-} mice. Future studies to elucidate the mechanisms for decreased adiposity and altered whole-body glucose homeostasis have the potential to uncover therapeutic options for patients with Wilson's disease, as well as for patients with metabolic disorders such as type 2 diabetes and fatty liver disease.

Methods

Animal Care. *Atp7b*^{-/-} (C57BL/6J × 129SvEv) mice (48) were backcrossed for 10 generations with C57BL/6J mice to generate *Atp7b*^{+/-} mice on a C57BL/6J background strain. Male *Atp7b*^{-/-} and WT cagemate/littermate controls for the study were obtained from heterozygous *Atp7b*^{+/-} mating cages. Mice were fed either a standard chow diet (Harlan Laboratories 2920X) or a 40% kcal from fat, 35% sucrose Western-type diet (Research Diets). Copper content of the chow and Western-type diet was 17.23 and 10 mg/kg, respectively. Diets and water were provided ad libitum, and mice were maintained on a 12-h light–dark cycle and euthanized at Zeitgeber Time 2–3. All experiments were performed under the guidelines detailed in the *Guide for the Care and Use of Laboratory Animals* (49), and animal experiments were approved by the Institutional Animal Care and Use Committee at Baylor College of Medicine (BCM).

Inductively Coupled Plasma–Optical Emission Spectrometry. Liver samples were processed as previously described (8).

Body Composition. Total fat and lean mass were measured on ad-libitum-fed mice at the end of the diet study using an EchoMRI Whole Body Composition Analyzer (Echo Medical Systems) located in the Mouse Metabolic Research Unit (MMRU) at the US Department of Agriculture/Agricultural Research Service (USDA/ARS) Children's Nutrition Research Center (CNRC) at BCM.

Plasma and Hepatic Lipids. Mice were fasted for 6 h prior to blood collection between 1:00 and 2:00 PM. Livers were dissected from mice in the ad-libitum-fed state. Plasma and liver triglycerides (Pointe Scientific), cholesterol (Pointe Scientific), and free fatty acids (BioVision) were measured following manufacturer protocols. Serum chemistry profiles (alanine transaminase, alkaline phosphatase, bilirubin, albumin, globulin) were performed in the Center for Comparative Medicine at BCM.

Histology. Liver samples were fixed in 10% formalin (for hematoxylin and eosin, PAS, and PAS-diastase staining) or frozen in Optimal Cutting Temperature compound for Oil Red O staining, and staining was performed at the Digestive Disease Core at BCM.

Indirect Calorimetry, Food Intake, and Activity. Indirect calorimetry, food intake, and activity measurements were performed in the MMRU at the USDA/ARS CNRC at BCM as previously described (50). To minimize the confounding effect of different body weights on energy expenditure (51), experiments were performed on chow-diet-fed mice, when mice were 12 wk old, prior to significant differences in body weight between genotypes. Age- and weight-matched littermates were singly housed and acclimated for 6 d in metabolic chambers. Subsequently, indirect calorimetry, food intake, and activity were measured over a 24-h period using an Oxymax/Comprehensive Lab Animal Monitoring System (Oxymax/CLAMS, Columbus Instruments). Data were acquired using the CLAMS data Examination Tool (CLAX, Columbus Instruments). RER and energy expenditure were calculated as previously described (50).

Whole-Body Glucose Homeostasis. Prior to intraperitoneal injection, mice were fasted for 6 h for GTT and ITT, or overnight for PTT. For GTT, 1.5 g/kg dextrose (Sigma); for ITT, 0.75 U/kg human insulin (Eli Lilly and Company); or for PTT, 1.0 g/kg sodium pyruvate (Sigma) was injected. Immediately prior and subsequent to injections, blood glucose was measured via glucometer (OneTouch) at time points shown. For GTT, blood was collected, and plasma insulin was measured using a Rat/Mouse Insulin ELISA kit (EMD Millipore). Hyperinsulinemic euglycemic clamp studies were performed at the Mouse Metabolomic and Phenotyping Core (MMPC) at BCM.

Protein Analysis. Western blot analysis on liver and gastrocnemius dissected in the ad-libitum-fed state was performed with 1:1,000 α-AMPK (23A3, Cell Signaling), phospho(T172)-α-AMPK (40H9, Cell Signaling), α-tubulin (ab-4074, Abcam), 36B4 (RPLP0) (Cell Signaling), and 1:50,000 secondary antibody.

Real Time-PCR. RNA was harvested from 100 mg of liver samples using TRIzol Reagent (Invitrogen), and synthesized cDNA (Invitrogen) was used as template for real-time PCR with SYBR Green reagent (Roche) on a 384-well LightCycler (Roche). Primers were designed with the Roche Universal Primer website. Reactions were normalized to 36B4 mRNA expression.

Metabolite Measurements. Six-month-old glycolytic and TCA cycle metabolites were measured in livers taken from ad-libitum-fed mice in the BCM Metabolomics Core. The extended protocol is provided in *SI Appendix*.

Microarray Analysis. RNA was harvested from male and female 3-mo-old *Atp7b*^{-/-} mice and WT controls with TRIzol Reagent (Invitrogen), followed with RNeasy kit (Qiagen). Microarray processing using a GeneChip Mouse 430 2.0 (Affymetrix) was performed in the Genomic and RNA Profiling Core at BCM. Data are available at the Gene Expression Omnibus database under accession no. GSE125637 (52). Datasets were analyzed as previously described (31).

Serum Growth/Differentiation Factor 15 Measurement. Serum from ad-libitum-fed mice was collected and analyzed using the Mouse/Rat GDF-15 Quantikine ELISA Kit (R&D Systems) per manufacturer protocol.

Statistical Analysis. Statistical analysis was performed with GraphPad Prism software (v7.0). Data are presented as mean \pm the SEM, and $P < 0.05$ was considered statistically significant. Student's t test was used to compare differences between two groups. For multiple-group comparison, two-way ANOVA tests followed by Sidak's post hoc test were performed.

1. S. Lutsenko, N. L. Barnes, M. Y. Bartee, O. Y. Dmitriev, Function and regulation of human copper-transporting ATPases. *Physiol. Rev.* **87**, 1011–1046 (2007).
2. S. Lutsenko, E. S. LeShane, U. Shinde, Biochemical basis of regulation of human copper-transporting ATPases. *Arch. Biochem. Biophys.* **463**, 134–148 (2007).
3. G. V. Sarode *et al.*, Metabolomics profiles of patients with Wilson disease reveal a distinct metabolic signature. *Metabolomics* **15**, 43 (2019).
4. J. Xu *et al.*, 1H NMR-based metabolomics investigation of copper-laden rat: A model of Wilson's disease. *PLoS One* **10**, e0119654 (2015).
5. J. P. Hamilton *et al.*, Activation of liver X receptor/retinoid X receptor pathway ameliorates liver disease in *Atp7b*^{-/-} (Wilson disease) mice. *Hepatology* **63**, 1828–1841 (2016).
6. D. Huster *et al.*, High copper selectively alters lipid metabolism and cell cycle machinery in the mouse model of Wilson disease. *J. Biol. Chem.* **282**, 8343–8355 (2007).
7. P. A. Wilmarth *et al.*, A systems approach implicates nuclear receptor targeting in the *Atp7b*^{-/-} mouse model of Wilson's disease. *Metallomics* **4**, 660–668 (2012).
8. C. R. Wootton-Kee *et al.*, Elevated copper impairs hepatic nuclear receptor function in Wilson's disease. *J. Clin. Invest.* **125**, 3449–3460 (2015).
9. H. Nagasaka *et al.*, Relationship between oxidative stress and antioxidant systems in the liver of patients with Wilson disease: Hepatic manifestation in Wilson disease as a consequence of augmented oxidative stress. *Pediatr. Res.* **60**, 472–477 (2006).
10. H. Nagasaka *et al.*, Fatty liver and anti-oxidant enzyme activities along with peroxisome proliferator-activated receptors γ and α expressions in the liver of Wilson's disease. *Mol. Genet. Metab.* **107**, 542–547 (2012).
11. C. E. Mordaunt *et al.*, Epigenomic signatures in liver and blood of Wilson disease patients indicate hypermethylation of liver-specific enhancers. *Epigenetics Chromatin* **12**, 10 (2019).
12. D. Huster *et al.*, Consequences of copper accumulation in the livers of the *Atp7b*^{-/-} (Wilson disease gene) knockout mice. *Am. J. Pathol.* **168**, 423–434 (2006).
13. K. Johansen, G. Gregersen, Glucose intolerance in Wilson's disease. Normalization after treatment with penicillamine. *Arch. Intern. Med.* **129**, 587–590 (1972).
14. R. Krysiak, G. Handzlik-Orlik, B. Okopień, Endocrine symptoms as the initial manifestation of Wilson's disease. *Yale J. Biol. Med.* **85**, 249–254 (2012).
15. K. Bwanahali, M. Mbuyi, B. Kapita, Osteoarthritis, gout and arthritis rheumatoid in internal medicine in Kinshasa [in French]. *Rev. Rhum. Mal. Osteoartic.* **58**, 105–111 (1991).
16. J. E. Ayala *et al.*, NIH Mouse Metabolic Phenotyping Center Consortium, Standard operating procedures for describing and performing metabolic tests of glucose homeostasis in mice. *Dis. Model. Mech.* **3**, 525–534 (2010).
17. A. Méndez-Lucas *et al.*, PEPCK-M expression in mouse liver potentiates, not replaces, PEPCK-C mediated gluconeogenesis. *J. Hepatol.* **59**, 105–113 (2013).
18. A. Méndez-Lucas, P. Hyrššová, L. Novellademunt, F. Viñals, J. C. Perales, Mitochondrial phosphoenolpyruvate carboxykinase (PEPCK-M) is a pro-survival, endoplasmic reticulum (ER) stress response gene involved in tumor cell adaptation to nutrient availability. *J. Biol. Chem.* **289**, 22090–22102 (2014).
19. T. E. Roche, Y. Hiromasa, Pyruvate dehydrogenase kinase regulatory mechanisms and inhibition in treating diabetes, heart ischemia, and cancer. *Cell. Mol. Life Sci.* **64**, 830–849 (2007).
20. J. P. Hamilton *et al.*, Activation of LXR/RXR pathway ameliorates liver disease in *atp7b* (Wilson disease) mice. *Hepatology* (2015).
21. V. W. W. Tsai, Y. Husaini, A. Sainsbury, D. A. Brown, S. N. Breit, The MIC-1/GDF15-GFRAL pathway in energy homeostasis: Implications for obesity, cachexia, and other associated diseases. *Cell Metab.* **28**, 353–368 (2018).
22. L. Krishnamoorthy *et al.*, Copper regulates cyclic-AMP-dependent lipolysis. *Nat. Chem. Biol.* **12**, 586–592 (2016).
23. E. Aigner *et al.*, A role for low hepatic copper concentrations in nonalcoholic fatty liver disease. *Am. J. Gastroenterol.* **105**, 1978–1985 (2010).
24. V. Nobili *et al.*, Levels of serum ceruloplasmin associate with pediatric nonalcoholic fatty liver disease. *J. Pediatr. Gastroenterol. Nutr.* **56**, 370–375 (2013).
25. M. Song *et al.*, High fructose feeding induces copper deficiency in Sprague-Dawley rats: A novel mechanism for obesity related fatty liver. *J. Hepatol.* **56**, 433–440 (2012).
26. M. Song *et al.*, Modest fructose beverage intake causes liver injury and fat accumulation in marginal copper deficient rats. *Obesity (Silver Spring)* **21**, 1669–1675 (2013).
27. A. Muchenditsi *et al.*, Targeted inactivation of copper transporter *Atp7b* in hepatocytes causes liver steatosis and obesity in mice. *Am. J. Physiol. Gastrointest. Liver Physiol.* **313**, G39–G49 (2017).
28. H. Pierson *et al.*, The function of ATPase copper transporter ATP7B in intestine. *Gastroenterology* **154**, 168–180.e5 (2018).
29. C. Eimer *et al.*, A high-calorie diet aggravates mitochondrial dysfunction and triggers severe liver damage in Wilson disease rats. *Cell. Mol. Gastroenterol. Hepatol.* **7**, 571–596 (2019).
30. S. Ahmed, J. Deng, J. Borjigin, A new strain of rat for functional analysis of PINA. *Brain Res. Mol. Brain Res.* **137**, 63–69 (2005).
31. H. Zischka *et al.*, Liver mitochondrial membrane crosslinking and destruction in a rat model of Wilson disease. *J. Clin. Invest.* **121**, 1508–1518 (2011).
32. R. Krysiak, B. Okopień, Whipple's triad as a clinical manifestation of hepatolenticular degeneration. *Pol. Arch. Med. Wewn.* **117**, 53–55 (2007).
33. Y. Arakawa, M. Moriyama, Y. Arakawa, Liver cirrhosis and metabolism (sugar, protein, fat and trace elements). *Hepatol. Res.* **30S**, 46–58 (2004).
34. H. Y. Lin *et al.*, Increased hepatic steatosis and insulin resistance in mice lacking hepatic androgen receptor. *Hepatology* **47**, 1924–1935 (2008).
35. T. Kanda, O. Yokosuka, The androgen receptor as an emerging target in hepatocellular carcinoma. *J. Hepatocell. Carcinoma* **2**, 91–99 (2015).
36. B. Renga *et al.*, Glucocorticoid receptor mediates the gluconeogenic activity of the farnesoid X receptor in the fasting condition. *FASEB J.* **26**, 3021–3031 (2012).
37. D. G. Hardie, S. A. Hawley, J. W. Scott, AMP-activated protein kinase: Development of the energy sensor concept. *J. Physiol.* **574**, 7–15 (2006).
38. S. L. Choi *et al.*, The regulation of AMP-activated protein kinase by H(2)O(2). *Biochem. Biophys. Res. Commun.* **287**, 92–97 (2001).
39. M. Lee *et al.*, Critical roles of AMP-activated protein kinase in the carcinogenic metal-induced expression of VEGF and HIF-1 proteins in DU145 prostate carcinoma. *Biochem. Pharmacol.* **72**, 91–103 (2006).
40. Y. Wu, M. Viana, S. Thirumangalathu, M. R. Loeken, AMP-activated protein kinase mediates effects of oxidative stress on embryo gene expression in a mouse model of diabetic embryopathy. *Diabetologia* **55**, 245–254 (2012).
41. Y. Shang *et al.*, Targeted expression of uncoupling protein 2 to mouse liver increases the susceptibility to lipopolysaccharide/galactosamine-induced acute liver injury. *Hepatology* **50**, 1204–1216 (2009).
42. K. D. Chavin *et al.*, Obesity induces expression of uncoupling protein-2 in hepatocytes and promotes liver ATP depletion. *J. Biol. Chem.* **274**, 5692–5700 (1999).
43. A. Lachmann *et al.*, ChEA: Transcription factor regulation inferred from integrating genome-wide ChIP-X experiments. *Bioinformatics* **26**, 2438–2444 (2010).
44. ENCODE Project Consortium, The ENCODE (ENCyclopedia of DNA elements) project. *Science* **306**, 636–640 (2004).
45. ENCODE Project Consortium, A user's guide to the encyclopedia of DNA elements (ENCODE). *PLoS Biol.* **9**, e1001046 (2011).
46. B. F. Peake, S. M. Eze, L. Yang, R. C. Castellino, R. Nahta, Growth differentiation factor 15 mediates epithelial mesenchymal transition and invasion of breast cancers through IGF-1R-FoxM1 signaling. *Oncotarget* **8**, 94393–94406 (2017).
47. H. Ye *et al.*, Hepatocyte nuclear factor 3/fork head homolog 11 is expressed in proliferating epithelial and mesenchymal cells of embryonic and adult tissues. *Mol. Cell. Biol.* **17**, 1626–1641 (1997).
48. O. I. Buiakova *et al.*, Null mutation of the murine ATP7B (Wilson disease) gene results in intracellular copper accumulation and late-onset hepatic nodular transformation. *Hum. Mol. Genet.* **8**, 1665–1671 (1999).
49. National Research Council, *Guide for the Care and Use of Laboratory Animals* (National Academies Press, Washington, DC, ed. 8, 2011).
50. A. M. Nuotio-Antar, D. L. Hachey, A. H. Hasty, Carbenoxolone treatment attenuates symptoms of metabolic syndrome and atherogenesis in obese, hyperlipidemic mice. *Am. J. Physiol. Endocrinol. Metab.* **293**, E1517–E1528 (2007).
51. A. A. Butler, L. P. Kozak, A recurring problem with the analysis of energy expenditure in genetic models expressing lean and obese phenotypes. *Diabetes* **59**, 323–329 (2010).
52. C. R. Wootton-Kee, C. Coarfa, M. Robertson, Gene expression in wild type and *Atp7b*^{-/-} mice. Gene Expression Omnibus. <https://www.ncbi.nlm.nih.gov/geo/query/acc.cgi?acc=GSE125637>. Deposited 25 January 2019.